Chemical Geology 269 (2010) 339–349

Contents lists available at ScienceDirect

Chemical Geology

journal homepage: www.elsevier.com/locate/chemgeo

Tracing the origin of subduction components beneath the South East rift in the Manus Basin, Papua New Guinea

Sung-Hyun Park [a,*], Sang-Mook Lee [b,*], George D. Kamenov [c], Sung-Tack Kwon [d], Kyeong-Yong Lee [e]

[a] Korea Polar Research Institute, Incheon, Republic of Korea
[b] School of Earth and Environmental Sciences, Seoul National University, Seoul, Republic of Korea
[c] Department of Geological Sciences, University of Florida, Gainesville, FL32611, USA
[d] Department of Earth System Sciences, Yonsei University, Seoul, Republic of Korea
[e] Deep-Sea Research Program, Korea Ocean Research and Development Institute, Ansan, P.O. Box 29, Seoul, Republic of Korea

ARTICLE INFO

Article history:
Received 3 August 2008
Received in revised form 9 October 2009
Accepted 16 October 2009

Editor: B. Bourdon

Keywords:
South East Rift
Manus Basin
Early subduction
Subduction component
Reactivation of ancient
subduction components

ABSTRACT

The Manus Basin to the northeast of Papua New Guinea is an actively spreading/rifting back-arc basin in the Bismarck Sea located between the inactive Manus-Kilinailau trench on the Pacific-plate side and the active New Britain trench on the Solomon-plate side. Spreading/rifting in the Manus Basin takes place in the last 0.78 Myr or so. We present major and trace elements, and Sr–Nd–Pb isotope compositions of rock samples taken from the South East Rift (SER) at the eastern end of the Manus Basin. The strong enrichment of Pb and LILE (large ion lithophile elements) relative to HFSE (high field strength elements) and REE (rare earth elements) in the SER lava is also quite similar to other island arc lavas, suggesting that substantial amount of subduction components were present in its source mantle. To investigate the origin of the subduction components in SER lavas, we compare the geochemical data of SER lavas to published data from New Britain Arc (NBA) and Tabar–Lihir–Tanga–Feni (TLTF) island chain. The volcanism in NBA is related to presently active subduction of the Solomon slab, whereas the TLTF volcanism is located in the forearc area of New Ireland arc which was formed during a former subduction of the Pacific slab. In other words, the NBA and TLTF lavas were influenced by subduction components from the present and former subduction, respectively. We argue that the subduction components in SER lava were incorporated in the mantle lithosphere during the active arc volcanism on New Ireland because the amount of the subduction component in SER decreases with increasing in distance from New Ireland. On the other hand, no relationships are found with respect to New Britain. The Sr–Nd–Pb isotopes indicate that SER lavas contain little sediment component and less amount of fluid component derived from altered oceanic crust compared to the TLTF lavas. This is probably due to the fact that SER is located in backarc settings in contrast to TLTF which is located in forearc setting with respect to the Pacific slab. Thus it is likely that the sediment was removed from the slab in the forearc and/or arc areas, and therefore little or none was introduced in the backarc mantle, which is the source region for SER magmas at present. Fluid derived from altered oceanic crust also may have made its way into the sub-forearc region more effectively than backare region by shallow dehydration process.

1. Introduction

Several recent studies have shown that, in addition to components derived from present-day subduction, ancient subduction components also can play an important role in the geochemistry of backarc basin lavas (Pearce et al. 2005; Langmuir et al., 2006; Pearce et al., 2006). For example, Pearce et al. (2006) revealed presence of ancient subduction components in some backarc basins, such as Mariana Trough and East Scotia Sea. In light of these developments, it is important to discriminate the ancient from present-day subduction components in order to improve the understanding of the geological processes in active back-arc systems. Furthermore, the transport mechanism of the subduction components into the present melting regime should be explored.

The South East Rift (SER) is an active volcanic region located in the eastern end of the Manus Basin, which comprises the eastern section of the Bismarck Sea (Fig. 1). The region surrounding the study area is a part of the Melanesian Borderland, where complex tectonic interactions have occurred between the Pacific and Indo-Australian plates during the last 50 million years (Kroenke, 1984). In the Oligocene, the subduction of the Pacific plate into the Manus-Kilinailau trench was terminated by the collision of the Ontong Java Plateau. The collision produced a new subduction zone with an opposite polarity farther to the south along the present-day New Britain trench (Lee and Ruellan, 2006). Later the Manus Basin opened up as a backarc basin in several

* Corresponding authors. Tel.: +82 32 260 6119; fax: +82 32 260 6243.
E-mail addresses: shpark314@kopri.re.kr (S.-H. Park), smlee@snu.ac.kr (S.-M. Lee).

0009-2541/$ – see front matter © 2009 Elsevier B.V. All rights reserved.
doi:10.1016/j.chemgeo.2009.10.008

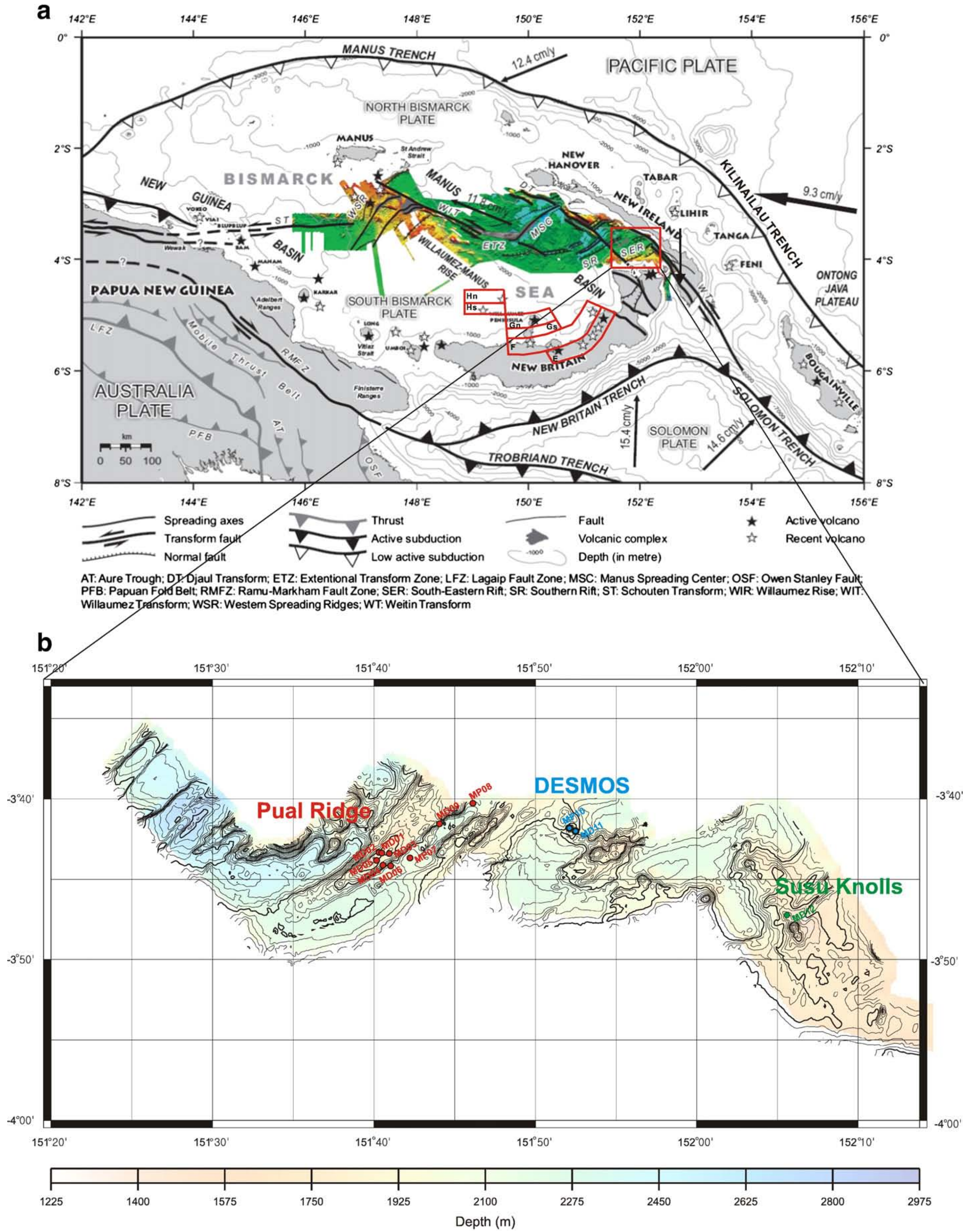
a
MANUS TRENCH
PACIFIC PLATE
12.4 cm/y
NORTH BISMARCK PLATE
MANUS
St Andrew Strait
NEW HANOVER
TABAR
KILINAILAU TRENCH
9.3 cm/y
BISMARCK
NEW GUINEA
MANUS
WSR
WIT
11.8 cm/y
DT
MSC
ETZ
SR
SER
NEW IRELAND
LIHIR
TANGA
FENI
ONTONG JAVA PLATEAU
ST
BASIN
WILLAUMEZ-MANUS RISE
SEA
BASIN
PAPUA NEW GUINEA
SOUTH BISMARCK PLATE
Hn
Hs
Gn
Gs
F
E
NEW BRITAIN
BOUGAINVILLE
AUSTRALIA PLATE
LFZ
Mobile Thrust Belt
RMFZ
PFB
AT
OSF
NEW BRITAIN TRENCH
15.4 cm/y
SOLOMON PLATE
14.6 cm/y
SOLOMON TRENCH
TROBRIAND TRENCH
km
0 50 100
142°E 144°E 146°E 148°E 150°E 152°E 154°E 156°E
0° 2°S 4°S 6°S 8°S
Spreading axes
Transform fault
Normal fault
Thrust
Active subduction
Low active subduction
Fault
Volcanic complex
Depth (in metre)
Active volcano
Recent volcano
AT: Aure Trough; DT: Djaul Transform; ETZ: Extentional Transform Zone; LFZ: Lagaip Fault Zone; MSC: Manus Spreading Center; OSF: Owen Stanley Fault; PFB: Papuan Fold Belt; RMFZ: Ramu-Markham Fault Zone; SER: South-Eastern Rift; SR: Southern Rift; ST: Schouten Transform; WIR: Willaumez Rise; WIT: Willaumez Transform; WSR: Western Spreading Ridges; WT: Weitin Transform
b
151°20' 151°30' 151°40' 151°50' 152°00' 152°10'
-3°40' -3°50' -4°00'
Pual Ridge
DESMOS
Susu Knolls
MP08
MP09
MD01
MD02
MD05
MP03
MP07
MD06
MP10
MP11
MP12
1225 1400 1575 1750 1925 2100 2275 2450 2625 2800 2975
Depth (m)

stages from east to west between the two trenches, one active and the other inactive (Lee and Ruellan, 2006).

Given the unusual tectonic history of this region, it is possible that the traces of the ancient Pacific plate subduction may still be present in the volcanic rocks of the Manus Basin. However, most of the previous petrologic studies have focused on the effects of the present-day subduction along the New Britain trench (e.g., Taylor and Martinez, 2003; Sinton et al., 2003) and have given little consideration on the effects of an earlier subduction. We envisage that the SER, an active volcanic region close to the Manus-Kilinailau trench, is one of the ideal places to look for the possible effects of early subduction because it is located between the young and old trenches (Fig. 1).

In this paper, we present new major and trace element and Sr–Nd–Pb isotopic data obtained from SER lavas and compare them with existing data from the New Britain Arc (NBA) and Tabar–Lihir–Tanga–Feni (TLTF) in order to explore the origin of subduction components in the SER. Previous studies show that while the NBA lava retains the geochemical characteristics of the subduction components from the present subduction (Woodhead et al., 1998), the TLTF lava carries those of early subduction (Kennedy et al., 1990; McInnes and Cameron, 1994; Stracke and Hegner, 1998; McInnes et al., 2001; Kamenov et al., 2008). At present the NBA is the active volcanic front of the active subduction of the Solomon slab, and this was shown from the analysis of Quaternary volcanism in NBA which contains the subduction components derived from the Solomon slab (Woodhead et al., 1998). The TLTF, on the other hand, represent the recent volcanism caused by rifting in the fore-arc region of New Ireland which was the volcanic front of early Pacific-slab subduction (Fig. 1). It is thought that TLTF mantle source was metasomatized during the early subduction episode (McInnes and Cameron, 1994) and the lavas geochemistry indicates strong control by subducted slab with Pacific affinity (Kamenov et al. 2008). Our analysis of the SER lava may provide clues to the origin of the subduction components and some insights into the transport mechanism of the subduction components in the mantle wedge.

2. Tectonic setting, sampling and analytical methods

2.1. Tectonic Setting and Sampling

According to recent detailed reconstruction of the Bismarck Sea by Lee and Ruellan (2006), the northern New Guinea region is thought to have developed from two lines of arcs, the Outer and Inner Melanesian arcs, somewhat similar to the present-day configuration of Solomon Island and Bougainville to the east. The proto-New Britain and proto-New Ireland were considered to be side-by-side in the Outer Melanesian Arc at this time. The collision of Finisterre-Huron Range with northern New Guinea around 3.0–3.7 Ma (Abbott et al., 1994) initiated the opening of the Bismarck Sea. The opening then caused the proto-New Britain to rotate to its present position south of New Ireland which began with the formation of the New Guinea Basin in the west (Lee and Ruellan, 2006) and only in the last 0.78 Myr or so (Martinez and Taylor, 1996) did rifting and seafloor spreading takes place in the Manus Basin.

Evidences that the Bismarck Sea opened from west to east in a highly oblique manner include GPS observations (Wallace et al., 2004), sediment thickness data, and the general shape and configuration of the Bismarck Sea (Lee and Ruellan, 2006). The opening of the Bismarck Sea within the last 3.0–3.7 Myr caused New Britain, which initially was along the Manus trench, to rotate and Solomon plate subduction was initiated. However, it remains unclear how much of the New Britain is the result of volcanic construction along the Outer Melanesian Arc, prior to the opening of the Bismarck Sea, and how much of the construction is the result of volcanism related to Solomon plate subduction.

The Manus Basin contains four extensional zones: SER in the east, South Rift (SR) in the south, MSC and the Extensional Transform Zone (ETZ) in the middle, separated by the Willaumez, Djaul, and Weitin faults (Fig. 1; Taylor et al., 1994; Martinez and Taylor, 1996). According to Martinez and Taylor (1996), the SER extension between the Djaul and Weitin transform faults (Fig. 1a) is accommodated by a series of *en echelon*, sinuous rift zones. The SER includes several volcanic constructional features, including Pual and SuSu Knolls (Fig. 1b). The extensive lava fields and high sonar reflectivity associated with them indicate that these areas are sites of recent volcanic activity.

The samples used in this study were obtained during a cruise onboard R/V *Onnuri* in 1999. The cruise included multi-beam bathymetric mapping, and collection of gravity and magnetic data. A total of 9 dredges and 3 piston cores were conducted in three areas where hydrothermal activity was previously observed (e.g., Binns and Scott, 1993; Gena et al., 1997: Pual Ridge, DESMOS Caldera and SuSu Knolls, Fig. 1b). Sampling locations are shown in Fig. 1b. From dredge and piston core samples, we chose fresh-looking rock samples for analyses. Most of the samples from Pual Ridge and SuSu Knoll were glass, but DESMOS samples were aphyric microcrystalline pillow lava. SuSu Knolls samples contain very small amounts of plagioclase phenocrysts.

2.2. Analytical methods

Major and trace elements analyses were done at Korea Ocean Research and Development Institute. Major element analysis was performed by X-ray fluorescence (XRF) spectrometry (Phillips Model, PW1450) on glass beads made with ultra-pure lithium tetra-borate ($LiBO_4$). Trace elements were analyzed by inductively coupled plasma source mass spectrometry (ICP-MS, PQII, VG element Co.) and ICP-atomic emission spectrometry (ICP-AES, Optima 3300DV, Perkin Elmer) with HNO_3-diluted solutions after prior dissolution with mixture of HNO_3, $HClO_4$, and HF in pressurized Teflon vessels. Sr–Nd isotopic ratios were measured using VG354 thermal ionization mass spectrometer at the Institute of Geology and Geophysics in Beijing, China. $^{87}Sr/^{86}Sr$ and $^{143}Nd/^{144}Nd$ ratios were normalized to $^{86}Sr/^{88}Sr = 0.1194$ and $^{146}Nd/^{144}Nd = 0.7219$, respectively. Replicate analysis of NIST SRM-987 and La Jolla standards gave $^{87}Sr/^{86}Sr = 0.710208 \pm 0.000009$ (N = 10) and $^{143}Nd/^{144}Nd = 0.511826 \pm 0.000008$ (N = 12), respectively. Total blanks averaged 0.2 ng for Sr, 0.05 ng for Nd.

Pb isotopes were analyzed using multi-collector ICP-MS (Nu Plasma, UK) at the University of Florida, following methods described in Kamenov et al. (2008). The Pb isotope data are relative to the following values of NBS 981: $^{206}Pb/^{204}Pb = 16.937$ (+/−0.004, 2σ), $^{207}Pb/^{204}Pb = 15.490$ (+/−0.003, 2σ), and $^{208}Pb/^{204}Pb = 36.695$ (+/−0.009, 2σ). Procedural blank processed together with the samples showed less than 20 pg Pb. The analytical results are in Table 1.

3. Results

3.1. Major and trace elements

The TAS diagram (Total Alkalis versus Silica, Fig. 2a) indicates that Pual Ridge lavas have a large compositional variation from basaltic

Fig. 1. a. Tectonic setting of the Manus Basin. Three major transform faults (Wilaumaz, WIT; Djaul, DT; Weitin, WT) bound four extensional zones in the Manus Basin: SER in the east, Manus spreading center (MSC) and the extensional transform zone (ETZ). New Britain Arc in the south of Manus Basin. (Fig. 1a, modified from Lee and Ruellan, 2006). Volcanic zones from E to Hn in New Britain Arc defined by Johnson (1977) and, Woodhead and Johnson (1993) are shown for reference. b. Bathymetric map and sampling locations (MD: Dredges, MP: Piston core) along SER. The contours are drawn at 50 m intervals.

Table 1
Major and trace element concentrations, and isotope ratios of SER lava.

Sample	Pual Ridge												
	MD01-1	MD01-2	MD01-3	MD01-4	MD01-5	MD02-1	MD02-2	MD03-1	MD03-2	MD03-3	MD04-1	MD04-2	MD05-1
SiO_2	69.89	69.78	64.84	65.63	65.26	69.31	68.29	69.10	68.75	69.16	70.45	69.86	67.57
TiO_2	0.61	0.60	0.79	0.80	0.81	0.63	0.62	0.61	0.61	0.59	0.61	0.60	0.64
Al_2O_3	13.90	13.86	14.69	14.77	14.63	14.12	13.76	13.63	13.73	13.73	13.83	13.88	13.84
FeO	4.34	5.06	5.73	5.57	5.83	4.43	4.41	4.27	4.24	4.13	4.27	4.24	4.96
MnO	0.13	0.15	0.16	0.15	0.15	0.13	0.13	0.13	0.12	0.12	0.12	0.13	0.15
MgO	0.91	1.04	1.90	1.79	1.92	0.93	0.93	0.88	0.84	0.84	0.87	0.88	1.76
CaO	3.07	3.56	4.57	4.49	4.63	3.12	3.12	3.01	2.97	2.92	3.04	3.01	3.78
Na_2O	4.91	4.88	4.45	4.42	4.49	4.84	4.97	4.88	4.89	4.75	4.77	4.93	4.65
K_2O	1.72	1.72	1.45	1.29	1.34	1.75	1.76	1.75	1.76	1.82	1.83	1.83	1.64
P_2O5	0.12	0.12	0.25	0.26	0.25	0.13	0.13	0.12	0.13	0.13	0.12	0.12	0.15
Total	99.60	100.79	98.81	99.17	99.33	99.38	98.12	98.38	98.04	98.19	99.92	99.48	99.14
Mg#	29.28	29.01	39.68	38.84	39.53	29.31	29.37	29.08	28.23	28.66	28.66	29.19	41.31
V	14.7	16.5	68.5	70.3	68.9	17.7	17.3	16.6	15.5	16.8	15.2	16.1	33.6
Cu	18	19	28	28	28	19	20	20	19	19	20	20	19
Zn	70	71	81	84	81	75	76	74	77	75	75	75	78
Sr	266	252	344	327	338	276	237	267	264	255	251	248	301
Y	27	24	25	24	24	25	20	28	27	24	26	22	27
Zr	104	102	80	83	82	109	110	109	112	111	115	111	100
Nb	2.15	1.89	1.77	1.67	3.12	1.63	2.05	2.28	2.50	2.15	2.40	2.66	1.60
Cs	0.48	0.48	0.36	0.38	0.39	0.57	0.49	0.48	0.48	0.49	0.50	0.49	0.45
Ba	320	314	268	258	269	340	324	330	339	331	343	338	317
La	8.59	8.44	7.46	7.87	8.10	11.26	9.00	8.16	8.76	8.69	8.91	8.82	8.16
Ce	20.11	19.71	17.67	17.82	18.78	24.68	20.69	19.62	20.44	20.23	20.23	20.34	18.94
Pr	2.82	2.79	2.49	2.55	2.68	3.47	2.92	2.73	2.84	2.83	2.85	2.85	2.65
Nd	13.72	13.59	12.73	12.80	13.34	16.52	14.23	13.44	13.87	13.75	13.96	13.84	13.10
Sm	3.55	3.48	3.34	3.32	3.46	4.21	3.72	3.53	3.61	3.61	3.61	3.56	3.40
Gd	4.20	4.13	3.95	3.99	4.10	4.94	4.33	4.12	4.28	4.29	4.22	4.25	4.04
Tb	0.74	0.71	0.69	0.68	0.70	0.84	0.75	0.72	0.73	0.74	0.74	0.72	0.68
Dy	4.87	4.83	4.47	4.45	4.59	5.50	4.97	4.79	4.91	4.96	4.85	4.88	4.60
Ho	1.07	1.06	0.97	0.96	1.00	1.19	1.09	1.05	1.06	1.07	1.06	1.06	1.01
Er	3.36	3.38	3.00	2.96	3.04	3.72	3.37	3.29	3.26	3.32	3.33	3.32	3.12
Tm	0.52	0.52	0.46	0.46	0.48	0.57	0.53	0.52	0.52	0.53	0.52	0.52	0.49
Yb	3.55	3.49	3.12	3.08	3.17	3.95	3.59	3.58	3.48	3.60	3.56	3.54	3.35
Lu	0.55	0.57	0.49	0.48	0.49	0.61	0.58	0.56	0.56	0.56	0.57	0.56	0.53
Hf	3.48	3.51	2.86	2.76	2.79	3.57	3.57	3.56	3.57	3.57	3.54	3.55	3.20
Pb	4.87	4.58	3.79	3.92	3.85	4.67	4.83	5.17	4.67	4.55	4.69	4.85	4.36
Th	1.19	1.17	0.94	0.90	0.99	1.37	1.23	1.17	1.18	1.20	1.23	1.20	1.10
U	0.75	0.76	0.63	0.63	0.65	0.90	0.78	0.77	0.77	0.74	0.77	0.77	0.71
$^{87}Sr/^{86}Sr$	0.70372										0.70371		
$^{143}Nd/^{144}Nd$	0.51303										0.51309		
eNd	7.62721										8.88		
$^{206}Pb/^{204}Pb$	18.77										18.777		
$^{207}Pb/^{204}Pb$	15.533										15.536		
$^{208}Pb/^{204}Pb$	38.360										38.366		

Analytical result (M1 and M2) and recommended value (R) of AGV-1 were presented in the right-end of columns. The recommended values of AGV-1 are from U.S. Geological Survey Certificate of Analysis. $Mg\# = Mg/[Mg + Fe^{2+}] \times 100$ with 10% total Fe as Fe^{3+}. $^{143}Nd/^{144}Nd_{CHUR(0)} = 0.512638$.

andesite to dacite. AFM (Fig. 2b), and K_2O versus SiO_2 (Fig. 2c) diagrams indicate that SER lavas belong to medium-K calc-alkaline series. Their composition more closely resembles lavas from a typical island arc than that of back-arc spreading center.

The spider diagram normalized to N-MORB shows marked enrichment of Pb and LILE relative to HFSE and REE (Fig. 3a). Fig. 3a also shows a negative Nb anomaly relative to adjacent elements. REE patterns normalized to chondrite reveal a slight enrichment of LREE relative to HREE (Fig. 3b). Again these trace element patterns are typical of island arc lava (e.g., Gill, 1981; Pearce and Peate, 1995) rather than typical back-arc spreading lava (e.g. Fryer et al., 1981; Pearce et al., 2006). Sinton et al. (2003) also found that the geochemistry of SER lavas to be similar to that of typical island arc lava.

Major oxides versus MgO variation diagrams resemble fractional crystallization trends (Fig. 4a–f), indicating olivine, clinopyroxene and plagioclase as major fractionating minerals. Al_2O_3 decrease more rapidly when MgO < 2 wt.%, suggesting a strong plagioclase control at this stage. In addition, accessory minerals also appear to have been precipitated during the fractionation of the SER lava. For example, Fig. 4c and e shows that FeO, TiO_2 and P_2O_5 decrease below 3.5 wt.% MgO, suggesting that Ti-magnetite and apatite joined in as fractionating minerals.

3.2. Radiogenic isotopes

The SER isotope data are plotted in Fig. 5 together with those from the MSC (Sinton et al., 2003), NBA (Woodhead et al., 1998) and TLTF (Stracke and Hegner, 1998 and Kamenov et al., 2005). In the SER lava, $^{87}Sr/^{86}Sr$ varies from 0.7036 to 0.7040 and $^{143}Nd/^{144}Nd$ from 0.512994 (εNd: +6.2) to 0.513161 (εNd: +10) (Table 1; Fig. 5a). The SER lava is higher in $^{87}Sr/^{86}Sr$ compared to the MSC and NBA lava, although their $^{143}Nd/^{144}Nd$ is similar. However, the SER lava is lower in $^{87}Sr/^{86}Sr$ but higher in $^{143}Nd/^{144}Nd$ compared to the TLTF lava.

In the SER lava, $^{206}Pb/^{204}Pb$ varies from 18.773 to 18.792, $^{207}Pb/^{204}Pb$ from 15.531 to 15.542, and $^{208}Pb/^{204}Pb$ from 38.360 to 38.378 (Table 1; Fig. 5c and d). An important finding is that the SER lavas fall within the Pacific-type MORB field in the $^{208}Pb/^{204}Pb$ versus $^{206}Pb/^{204}Pb$ diagram whereas the MSC lavas plot in the Indian-type MORB field (Fig. 5c).

4. Discussion

The strong arc signatures such as the enrichment of Pb and LILE relative to HFSE and REE in the SER lava imply that a substantial amount of subduction components is present in the sub-SER mantle.

Table 1 (*continued*)

											DESMOS		
MD05-2	MD05-3	MD05-4	MD05-5	MD06-1	MD06-2	MD06-3	MP07-1	MP08-1	MD09-1	MD09-2	MP10-1	MD11-1	MD11-2
65.96	70.04	67.98	69.04	56.45	56.25	62.24	69.32	60.02	69.88	68.31	56.36	56.05	56.54
0.65	0.60	0.74	0.59	0.94	0.95	0.93	0.61	1.02	0.55	0.60	0.55	0.55	0.57
13.85	13.86	14.40	13.97	15.23	15.18	14.93	13.53	15.03	13.74	13.51	15.76	15.71	15.74
4.89	4.27	4.86	4.18	10.01	10.12	7.02	4.30	7.79	3.97	4.30	7.56	7.42	7.58
0.14	0.12	0.14	0.12	0.17	0.17	0.16	0.18	0.17	0.12	0.12	0.14	0.14	0.14
1.73	0.89	1.24	0.86	4.18	4.24	2.43	0.71	2.66	0.61	0.72	6.09	5.58	6.01
3.80	3.05	3.69	2.96	7.85	7.89	5.40	2.69	5.89	2.47	2.68	9.82	9.62	9.79
4.52	4.78	4.66	4.81	3.33	3.35	4.09	4.70	3.95	4.66	4.87	2.88	2.64	2.66
1.63	1.87	1.65	1.78	0.91	0.94	1.55	1.85	1.24	2.14	2.08	0.85	0.85	0.81
0.15	0.12	0.19	0.12	0.24	0.24	0.39	0.12	0.44	0.10	0.12	0.15	0.14	0.14
97.33	99.62	99.56	98.45	99.30	99.34	99.16	98.01	98.20	98.24	97.32	100.16	98.70	99.99
41.18	29.27	33.62	29.01	45.24	45.34	40.72	24.63	40.31	23.21	24.77	61.45	59.83	61.10
34.2	15.1	43.2	15.5	452	454	152	11.9	236	11.0	15.4	245	244	246
20	20	31	20	507	500	23	11	33	18	19	92	93	93
79	75	79	75	78	78	86	82	90	76	77	67	64	66
290	232	310	269	400	410	408	272	449	278	277	437	434	450
26	22	28	27	15	16	24	30	23	27	21	13	12	12
100	115	103	112	41	41	69	118	63	121	117	38	37	37
1.84	2.52	1.98	2.44	1.63	1.71	1.54	6.17	2.11	2.42	2.33	2.23	1.88	1.64
0.44	0.42	0.46	0.50	0.20	0.20	0.32	0.54	0.32	0.58	0.57	0.24	0.20	0.23
313	332	309	343	147	151	234	376	213	400	395	172	174	179
7.89	6.13	8.34	9.03	4.46	4.50	7.13	9.31	6.61	9.47	8.79	3.92	3.92	4.03
18.59	15.38	19.52	20.82	10.64	10.71	16.97	21.65	15.83	22.07	20.94	9.21	9.31	9.52
2.61	2.07	2.75	2.88	1.50	1.52	2.40	3.11	2.31	3.06	2.87	1.28	1.28	1.28
12.70	10.47	13.46	14.00	7.94	8.08	12.40	14.93	11.84	14.48	13.81	6.67	6.69	6.76
3.36	2.77	3.42	3.71	2.20	2.24	3.29	3.84	3.13	3.71	3.47	1.70	1.72	1.77
4.02	3.43	4.21	4.31	2.80	2.80	3.96	4.50	3.77	4.25	4.08	2.08	2.05	2.04
0.68	0.60	0.72	0.74	0.46	0.46	0.65	0.77	0.64	0.72	0.68	0.34	0.33	0.34
4.56	4.10	4.73	5.02	3.07	3.02	4.20	5.08	4.10	4.76	4.52	2.20	2.07	2.16
1.00	0.91	1.02	1.08	0.66	0.67	0.92	1.13	0.88	1.04	1.00	0.47	0.46	0.47
3.09	2.83	3.12	3.33	1.98	1.98	2.72	3.37	2.60	3.22	3.08	1.37	1.33	1.38
0.50	0.47	0.51	0.52	0.32	0.32	0.45	0.57	0.44	0.54	0.52	0.25	0.23	0.24
3.35	3.13	3.42	3.62	1.97	2.03	2.89	3.67	2.68	3.57	3.35	1.40	1.36	1.40
0.53	0.50	0.53	0.57	0.31	0.31	0.44	0.57	0.41	0.55	0.51	0.21	0.21	0.22
3.28	3.49	3.16	3.64	1.57	1.56	2.38	3.58	2.11	3.70	3.61	1.34	1.37	1.37
4.39	4.76	4.38	5.02	2.27	2.31	3.38	6.06	3.29	5.83	5.85	2.44	2.32	2.40
1.09	1.00	1.14	1.24	0.52	0.53	0.83	1.32	0.75	1.43	1.34	0.53	0.50	0.52
0.69	0.61	0.72	0.78	0.40	0.40	0.55	0.86	0.51	0.86	0.84	0.38	0.37	0.37
			0.70373		0.70365		0.70373	0.70363	0.70374		0.70383	0.70382	
			0.51308		0.51309		0.51302	0.51305	0.51307		0.51299	0.51313	
			8.68		8.76		7.35	7.98	8.43		6.94	9.62	
			18.782		18.779				18.760				
			15.540		15.542				15.531				
			38.378		38.378				38.342				

(*continued on next page*)

For example, Nd/Pb ratio of the SER lavas (~4) is much lower than that of typical MORB (depleted) mantle (~24; Hofmann et al., 1988; Miller et al, 1994; Class et al., 2000), suggesting that the majority of Pb is present as subduction components. Furthermore, a significantly higher Sr/Nd (~34) and Ba/La (~41) ratios of the SER lavas than those of N-MORB (Sr/Nd: 12.32; Ba/La: 2.52, Sun and McDonough, 1989) indicate that a substantial amount of Sr and Ba have also entered into the SER source via subduction processes.

As shown in Fig. 6, neither incompatible element ratios nor radiogenic isotopic ratios such as $^{87}Sr/^{86}Sr$ and $^{207}Pb/^{204}Pb$ show a clear trend as a function of MgO. The lack of correlation with MgO suggests that AFC (Assimilation and Fractional Crystallization) did not play an important role during the genesis of the SER lava. For example, if AFC had occurred, then $^{87}Sr/^{86}Sr$ should increase with decreasing MgO since the assimilation of wall rock became more significant with progress of fractional crystallization (DePaolo, 1981). Furthermore, the depletion of Nb relative to the adjacent elements in spider diagram (Fig. 3a) and N-MORB like Zr/Nb ratios (~37) particularly does not favor the presence of OIB component in the sub-SER mantle.

The presence of subduction components below the SER itself may be not surprising after all because this area lies between the two trenches: the inactive Pacific and active Solomon subduction zones (Fig. 1). Instead, what is intriguing is that as shown in Fig. 5 the Sr–Nd–Pb isotope compositions of the SER lavas do not very much overlap with the NBA and TLTF lavas which were strongly influenced by the subduction components originated from the Solomon and Pacific slab, respectively. In addition, it is interesting that the Pb isotope ratios of SER lavas do not show evidence of a simple mixing of the subduction components from NBA and TLTF lavas (Fig. 5).

4.1. Deviation of SER lavas from NBA systematic

A detailed inspection of the isotope and trace elements data suggests that the subduction components in SER did not originate from the Solomon slab. According to Woodhead and Johnson (1993) and Woodhead et al. (1998), the amount of subduction components decreases away from the Solomon trench. From this trend, they defined the geochemical zones of the NBA from E to H with increasing distance from the Solomon trench (Fig. 1). For example, their study shows that Ba/La, which is sensitive indicator of the amount of the subduction components (e.g. Taylor and Martinez, 2003), decreases

Table 1 (*continued*)

Sample	DESMOS				SuSu Knoll			AGV-1			
	MD11-3	MD11-4	MD11-5	MD11-6	M12-1	M12-2	M12-3	M1	M2	R	±
SiO_2	56.31	56.03	56.37	56.33	64.90	65.06	65.18	60.50		58.84	0.58
TiO_2	0.56	0.57	0.55	0.55	0.75	0.77	0.76	1.14		1.05	0.05
Al_2O_3	15.74	15.62	15.62	15.76	14.37	14.33	14.33	17.19		17.15	0.34
FeO	7.51	7.52	7.45	7.46	6.43	6.32	6.36	6.33		6.09	0.19
MnO	0.14	0.14	0.14	0.14	0.15	0.15	0.16	0.10		0.09	
MgO	5.99	5.87	5.85	5.89	1.80	1.76	1.78	1.52		1.53	0.09
CaO	9.87	9.70	9.55	9.50	4.80	4.78	4.89	5.04		4.94	0.14
Na_2O	2.62	2.65	2.61	2.65	4.25	4.28	4.25	4.44		4.26	0.12
K_2O	0.80	0.83	0.83	0.82	1.14	1.15	1.10	2.94		2.92	0.37
P_2O5	0.14	0.15	0.15	0.14	0.22	0.22	0.22	0.50		0.5	0.03
Total	99.67	99.08	99.11	99.25	98.82	98.81	99.05	99.70		97.37	
Mg#	61.23	60.70	60.85	61.01	35.69	35.56	35.71				
V	242	245	246	225	168	168	168	113	113	120	11
Cu	92	92	92	88	140	141	139	59	59	60	6
Zn	64	65	66	59	85	86	86	86	85	88	9
Sr	453	442	437	417	410	409	413	642	632	660	9
Y	12	12	12	11	21	21	21	13	13	20	3
Zr	37	37	37	35	62	62	63	204	203	227	18
Nb	1.22	1.03	1.22	1.52	2.19	2.14	2.12	11.22	11.3	15	
Cs	0.22	0.23	0.22	0.23	0.46	0.47	0.47	0.95	0.98	1.3	0.1
Ba	177	175	174	165	304	305	306	1228	1207	1230	16
La	3.99	4.06	4.07	3.99	5.38	5.36	5.22	29.4	29.5	38	2
Ce	9.34	9.55	9.47	9.27	13.01	12.97	12.76	54.1	54.7	67	6
Pr	1.27	1.31	1.31	1.28	1.87	1.92	1.84	6.57	6.67	7.6	
Nd	6.74	6.85	6.85	6.78	9.86	9.82	9.75	25.8	25.9	33	3
Sm	1.75	1.78	1.73	1.75	2.70	2.71	2.69	4.72	4.79	5.9	0.4
Gd	2.05	2.12	2.06	2.04	3.40	3.38	3.31	4.61	4.69	5	0.6
Tb	0.33	0.33	0.33	0.33	0.55	0.56	0.55	0.59	0.60	0.7	0.1
Dy	2.14	2.20	2.16	2.12	3.61	3.66	3.61	3.36	3.33	3.6	0.4
Ho	0.46	0.48	0.46	0.45	0.79	0.80	0.78	0.62	0.61		
Er	1.38	1.38	1.37	1.33	2.36	2.33	2.38	1.69	1.72	1.7	
Tm	0.24	0.23	0.23	0.23	0.39	0.40	0.41	0.28	0.29	0.34	
Yb	1.39	1.40	1.39	1.37	2.46	2.47	2.45	1.56	1.57	1.72	0.2
Lu	0.21	0.21	0.22	0.21	0.38	0.36	0.37	0.23	0.23	0.27	0.03
Hf	1.34	1.37	1.32	1.31	2.04	2.11	2.10	4.9	5.0	5.1	0.4
Pb	2.45	2.60	2.52	2.62	4.29	4.45	4.35	37.4	37.5	36	5
Th	0.53	0.52	0.51	0.50	0.64	0.63	0.65	6.14	6.18	6.5	0.5
U	0.37	0.37	0.38	0.34	0.44	0.44	0.44	1.97	1.98	1.92	0.15
$^{87}Sr/^{86}Sr$		0.70377	0.70388	0.70370	0.70405	0.70391	0.70384				
$^{143}Nd/^{144}Nd$		0.51310	0.51316	0.51309	0.51304	0.51305	0.51309				
eNd		9.07		8.81714	7.78327	7.99785	8.87566				
$^{206P}b/^{204}Pb$		18.775		18.78		18.785	18.792				
$^{207}Pb/^{204}Pb$		15.539		15.54		15.530	15.536				
$^{208}Pb/^{204}Pb$		38.369		38.37		38.364	38.376				

from E to H in the NBA lavas (Fig. 7). In addition, Pb isotopes also decrease from zones E to H (Fig. 5).

It is important to note that although the distance to the SER from the Solomon trench is similar to that of zone G (Sinton et al., 2003), the geochemical characteristics of the lavas differ substantially from those of zone G (Figs. 1 and 5). For example, the Ba/La ratios of SER lavas are higher than those of zone G and plot within the compositional range of zones E and F (Fig. 7a). These findings appear to indicate that the amount of subduction components in the SER is higher than zone G and may even be close to the amount in zone E although SER is farther away from the Solomon trench than zone E. Furthermore, $^{206}Pb/^{204}Pb$ of the SER is even more radiogenic than that of zone E, which is the closest zone to the Solomon slab (Fig. 5cd). We also notice that $^{87}Sr/^{86}Sr$ of the SER lavas is overall higher than the NBA lavas (Figs. 5b and 7b). Hence, if the subduction components in the SER did originate from the Solomon slab, it would be difficult to explain why the subduction components increase in the SER lava and why the Sr and Pb isotopic ratios in the SER lavas differ from those of the NBA.

It appears that the melting depth was not a major factor affecting the geochemical difference between the SER and NBA lavas. The low Dy/Yb of the SER (~1.3) and the NBA (~1.5) lavas indicates that the melting of two lavas took place at depth shallower than ~60 km, the upper limit of the garnet stability field, so their melting depths were not much different from one another. This is evident from the high Dy/Yb of > 1.8, which is a sensitive indicator of the residual garnet in the source region (e.g., Langmuir et al., 2006).

4.2. The source of the subduction components in SER lavas

If the subduction components below the SER did not originate from the Solomon slab, then they must have come from the Pacific slab. Fig. 7 shows that the Ba/La ratio and $^{87}Sr/^{86}Sr$ systematically decreases in the SER lavas with increasing distance away from the New Ireland, which was the volcanic front of early subduction of the Pacific slab. The variation in Ba/La ratio and $^{87}Sr/^{86}Sr$ suggests that the amount of subduction components in the SER lava vary as a function of distance from the New Ireland (Fig. 7; from SuSu Knoll to Pual ridge). The Pb/Nd ratio, another indicator of the amount of subduction components (e.g. Class et al., 2000), also exhibits a similar trend as that of the Ba/La ratio. Such changes in the ratios tend to favor the hypothesis that the subduction components in the SER lavas

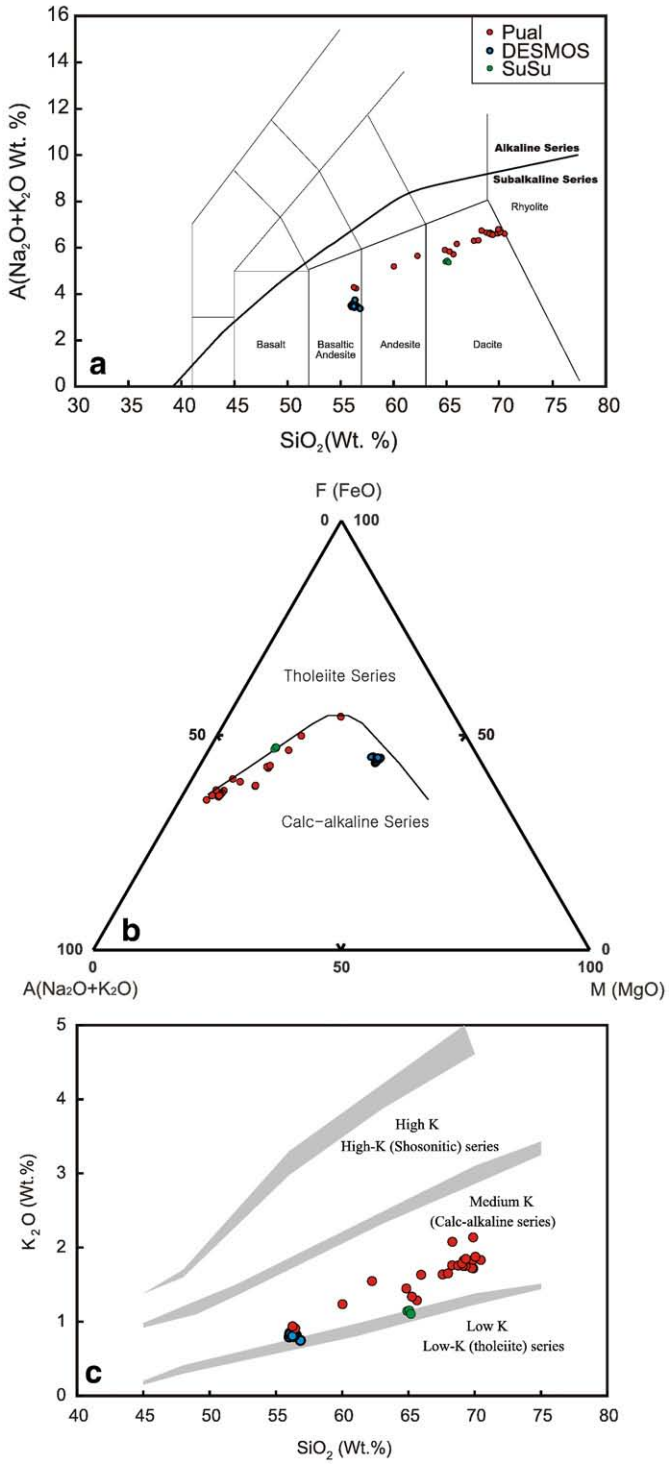

Fig. 2. Petrological diagrams of SER lavas. a. Plots of SER lava in Total Alkalis versus Silica diagram of Le Maitre et al. (1989). Dividing line between alkaline and subalkline is from Irvine and Baragar (1971). b. AFM diagram for SER lava. The dividing line between tholeiitic and calcalkline is from Irvine and Baragar (1971). The diagram shows that SER lavas belong to calc-alkline series. c. K_2O versus SiO_2 (wt.%) diagram for SER lava. Note that SER lava belong to medium K series. The shaded bands are the as described by Rickwood (1989).

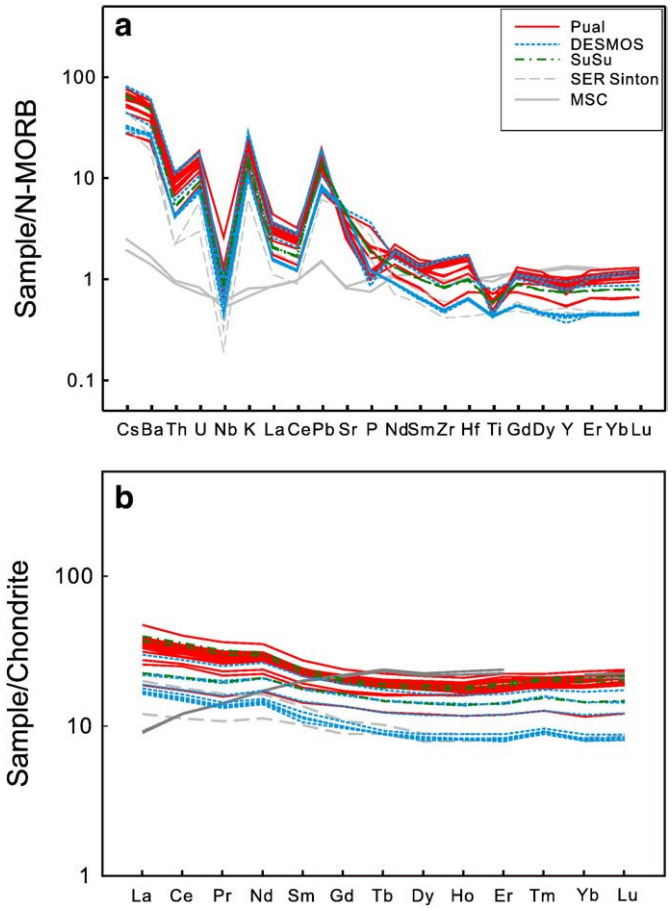

Fig. 3. a. Spider diagram for SER lavas normalized to N-MORB (Sun and McDonough, 1989). SER lava data from Sinton et al. (2003) are shown for comparison. b. Chondrite-normalized REE patterns of SER lava. The diagram also shows SER lava data from Sinton et al. (2003).

originated from the early subduction of the Pacific slab. Furthermore, it appears that SER lavas are isotopically more close to the TLTF lavas than the NBA (Fig. 5). For example, if we compare SER Pb isotopes data to the high-precision Pb isotope data from Lihir Island published by Kamenov et al.(2005), the difference becomes smaller as shown in Fig. 5c and d. It appears that for a given $^{206}Pb/^{204}Pb$ value, $^{87}Sr/^{86}Sr$ of SER lavas is closer to that of the TLTF than NBA (Fig. 5c).

Since the SER is close to New Ireland (within ~20 km from the shoreline), the mantle lithosphere beneath the SER region may contain the subduction component that affected the New Ireland as well. A number of previous studies have suggested that the mantle lithosphere in the region of the volcanic front can store a substantial amount of the subduction components (e.g., Pearce et al., 2006; Langmuir et al., 2006). Because SER is just beginning to rift, it is possible that the composition of magma is strongly influenced by low-melting components of the mantle lithosphere as well as the asthenospheric mantle (e.g. Pearce et al., 2005; Langmuir et al., 2006). According to Pearce et al. (2005), at the 'low melting point, enriched part' of the lithosphere can be melted to a low degree by the combined effects of heat transfer from the asthenosphere and decompression during initial stages of rifting.

Although the MSC is also close to New Ireland, there is little geochemical evidence for the presence of subduction components derived from the Pacific slab like that seen in the case of SER. The MSC is in a mature stage of seafloor spreading and therefore is different from the SER which is in initial rifting stage (Sinton et al., 2003). Thus ancient subduction components of MSC may have be melted out during seafloor spreading. If we consider that MSC began opening after 0.78 Ma (Martinez and Taylor, 1996), one could infer that it took less than 1 Myr to flush out the ancient subduction components.

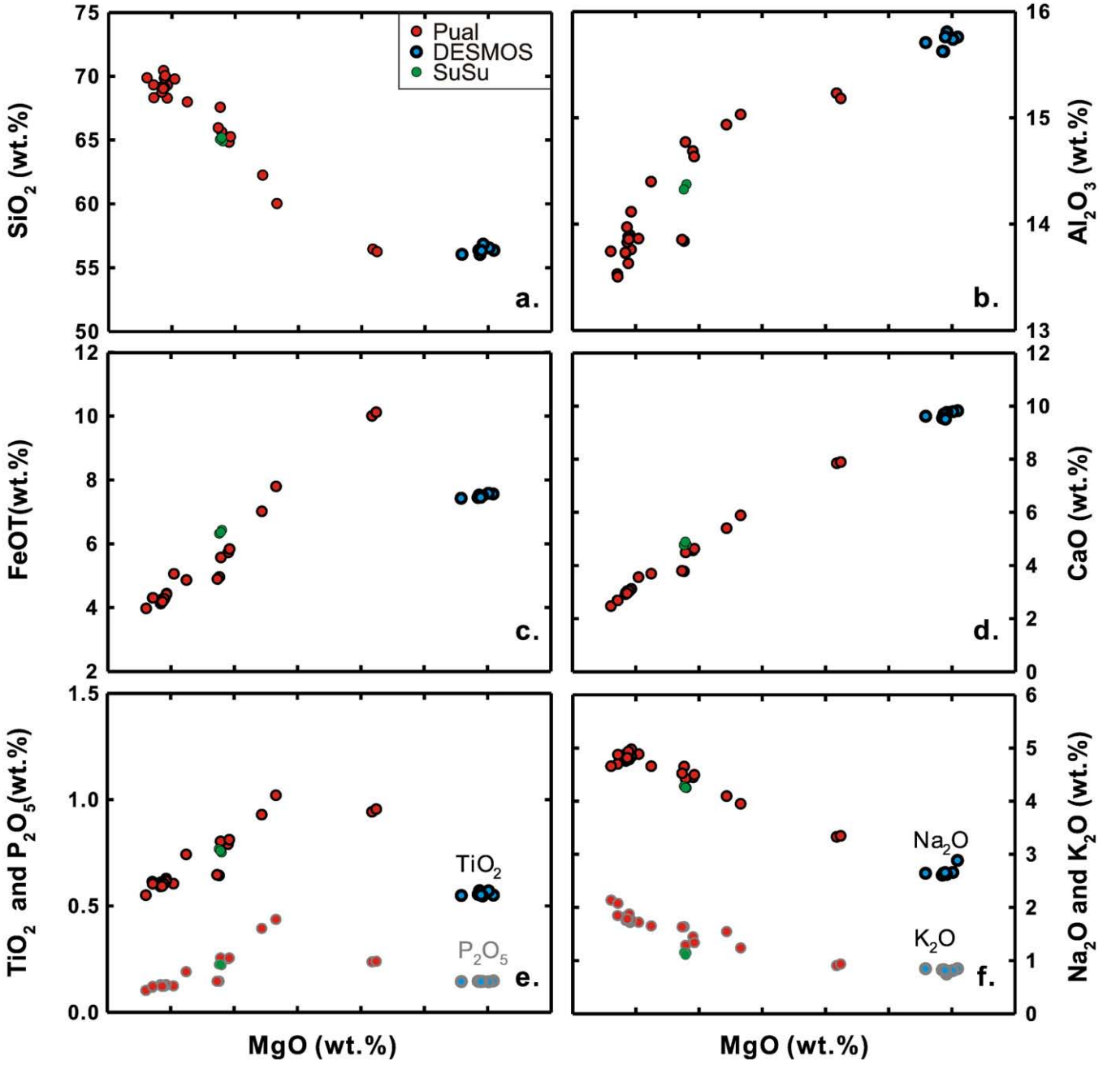

Fig. 4. Major oxides versus MgO diagrams.

4.3. Tectonic origin of isotopic differences between SER and TLTF lavas

Subduction components can enter into mantle wedge as sediment melt and fluid, and MORB fluid which are derived from subducted sediment and altered oceanic crust (altered MORB), respectively. Relative contributions of those components into lavas can be quantitatively evaluated using geochemical methods developed in several recent studies (e.g. Miller et al., 1994; Pearce and Peate, 1995; Class et al., 2000). Relative contributions of subduction components can give some insight into the tectonic process in the subduction zone. In this section, we attempt to quantify the relative contributions of subduction components in SER and TLTF in order to understand the cause of isotopic difference between SER and TLTF lavas.

Basically, the approach of Class et al. (2000) was used to calculate the contributions of each subduction components. Further details are described in Fig. 5. Fig. 5a illustrates that the contribution of sediment melt into SER source is negligible, but a small amount of sediment melt (0.2–0.3%) was incorporated in TLTF source. The fact that Pb isotopic ratios of SER are indistinguishable from those of Pacific MORB also precludes the involvement of sediment components in the SER source (Fig. 5cd).

Slightly elevated $^{87}Sr/^{86}Sr$ in SER lavas relative to a typical MORB (MSC) for given $^{143}Nd/^{144}Nd$ isotopes may be explained by the contribution of fluid from the altered oceanic crust (MORB fluid). Modeling shows that 0.5–2% of MORB fluid may have been added to the SER source (Fig. 5a). Low Nd/Pb ratios (~4) in SER lavas relative to mantle

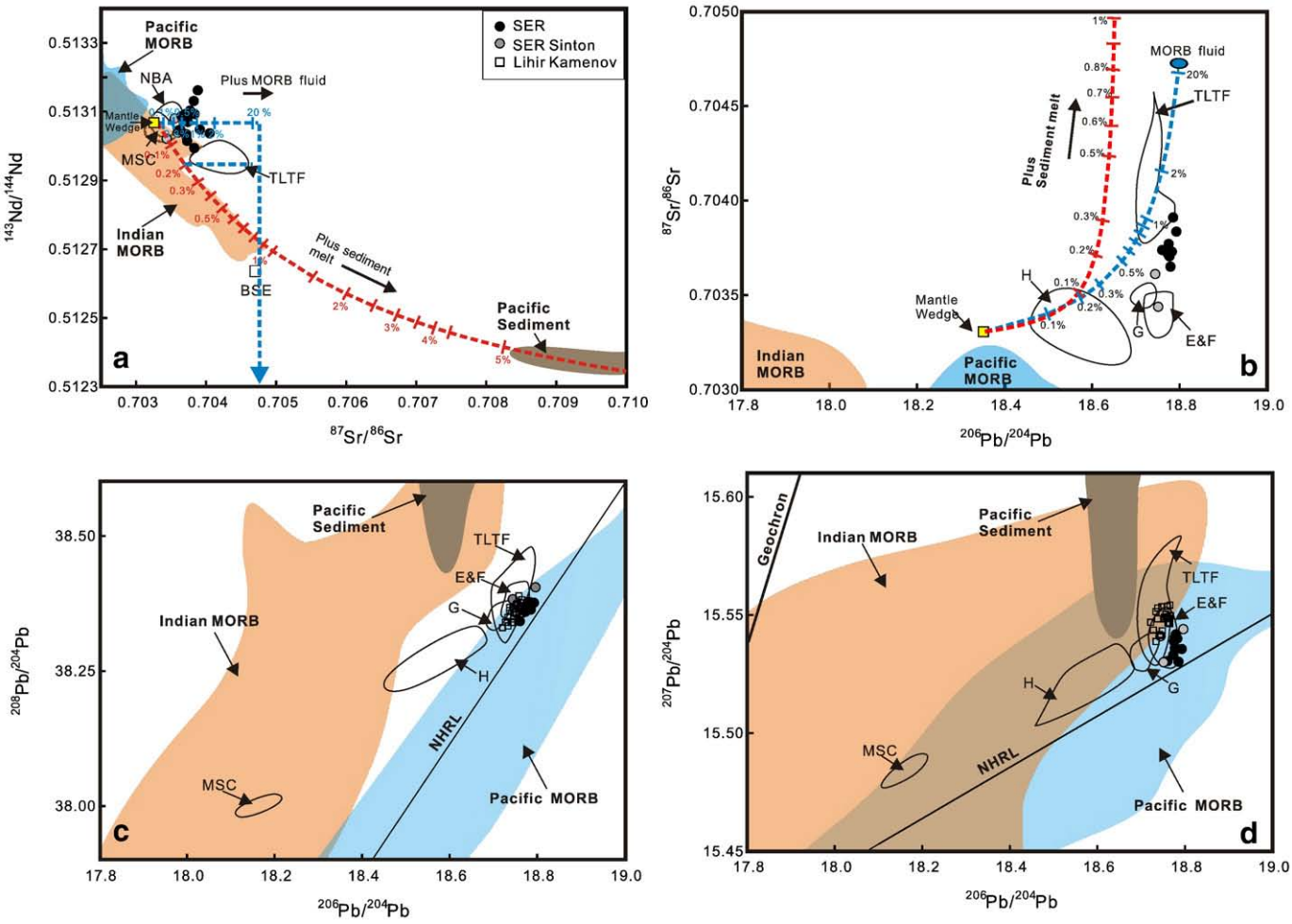

Fig. 5. Plots of Sr, Nd and Pb isotope data for SER lavas. SER data from Sinton et al. (2003) and high precision Pb isotope data of Lihir Island and surrounding seamounts from Kamenov et al. (2005) is also plotted. Area of MSC, NBA and TLTF are from Sinton et al. (2003), Woodhead et al. (1998) and, Stracke and Hegner (1998), respectively. Fields of Pacific and Indian MORB based on data from Hofmann (1997) and Hickey-Vargas et al. (1995). NHRL is from Hart (1984). Pacific sediment area was from Stracke and Hegner, (1998). BSE is Bulk Silicate Earth. a. $^{143}Nd/^{144}Nd$ versus $^{87}Sr/^{86}Sr$ diagram. b. $^{87}Sr/^{86}Sr$ versus $^{206}Pb/^{204}Pb$ diagram. c. $^{208}Pb/^{204}Pb$ versus $^{206}Pb/^{204}Pb$ diagram. d. $^{207}Pb/^{204}Pb$ versus $^{206}Pb/^{204}Pb$ diagram. Pacific sediment (Othman et al., 1989), recycled oceanic crust (Sun and McDonough, 1989) and depleted mantle (Salters and Stracke, 2004) were used as reference composition. Sr isotope for recycled oceanic crust was from Staudigel et al.(1995). Pb isotope composition for recycled oceanic crust is from Pacific MORB. Sr–Nd–Pb isotopes of mantle wedge from MSC. We used same modeling parameters listed in Class et al. (2000) to calculate the sediment melt, sediment fluid and MORB fluid from the sediment and altered MORB. Residual rutile was assumed for the calculation of sediment melt composition. This is because Nb/Th ratios of TLTF lavas is lower than that of normal sediment at given $^{143}Nd/^{144}Nd$ (Class et al., 2000).

value (~20) without increasing of $^{207}Pb/^{204}Pb$ strongly support the involvement of MORB fluid in SER lava sources (Miller et al., 1994).

TLTF lavas source also may have been influenced by MORB fluid as well as sediment melt. Fig. 5a shows that TLTF lavas deviate from mixing curve between mantle wedge and sediment melt, suggesting that some fluid component may have affected the TLTF source (Fig 5a). Fig. 5b shows that the Sr–Pb isotopic variations of SER and TLTF lavas can be better explained by mixing between the mantle wedge and MORB fluid rather than mixing of sediment melt and fluid. This suggests that the variation of Sr and Pb is controlled by the contribution of MORB fluid. It is also worth to note that TLTF source have more MORB fluid than SER source (Fig. 5b).

In summary, the amount of sediment melt is negligible in SER source. However, a small amount of sediment melt component is present in the TLTF source. MORB fluid is present both SER and TLTF, source regions, but its amount is higher in latter. These differences between the SER and TLTF lavas might be due to their tectonic setting; the SER is located in the backarc basin while the TLTF is in the forearc region. The mantle below the forearc is probably enriched in sediment components and MORB fluid relative to the mantle below the backarc basin (e.g. Kamenov et al. 2008). According to Kamenov et al. (2008), during the active subduction of the Pacific slab, fluids which are released from the sedimentary portion of the slab become metasomatized in the mantle below the New Ireland. This process may act as a hot "filter-press" that efficiently extracts the geochemical signature associated with the sedimentary portion of the slab. If such mechanism did occur, then most of the sediment will be left in the fore-arc mantle, and the mantle under the SER would be virtually free of subducted sediment component. Possibly, MORB fluid might be more effectively supplied into sub-forearc than backarc by shallow dehydration process from the subducting slab.

5. Conclusions

A strong enrichment of Pb and LILE relative to HFSE and REEs in the SER lavas suggest that a substantial amount of subduction components are present in the mantle source of the SER lava. To examine the source of the subduction components contained within the SER lavas, we compared the Sr–Nd–Pb isotopes and trace elements data of SER with those of the NBA and TLTF lavas, which we consider to represent the geochemical characteristics of the subduction components from the

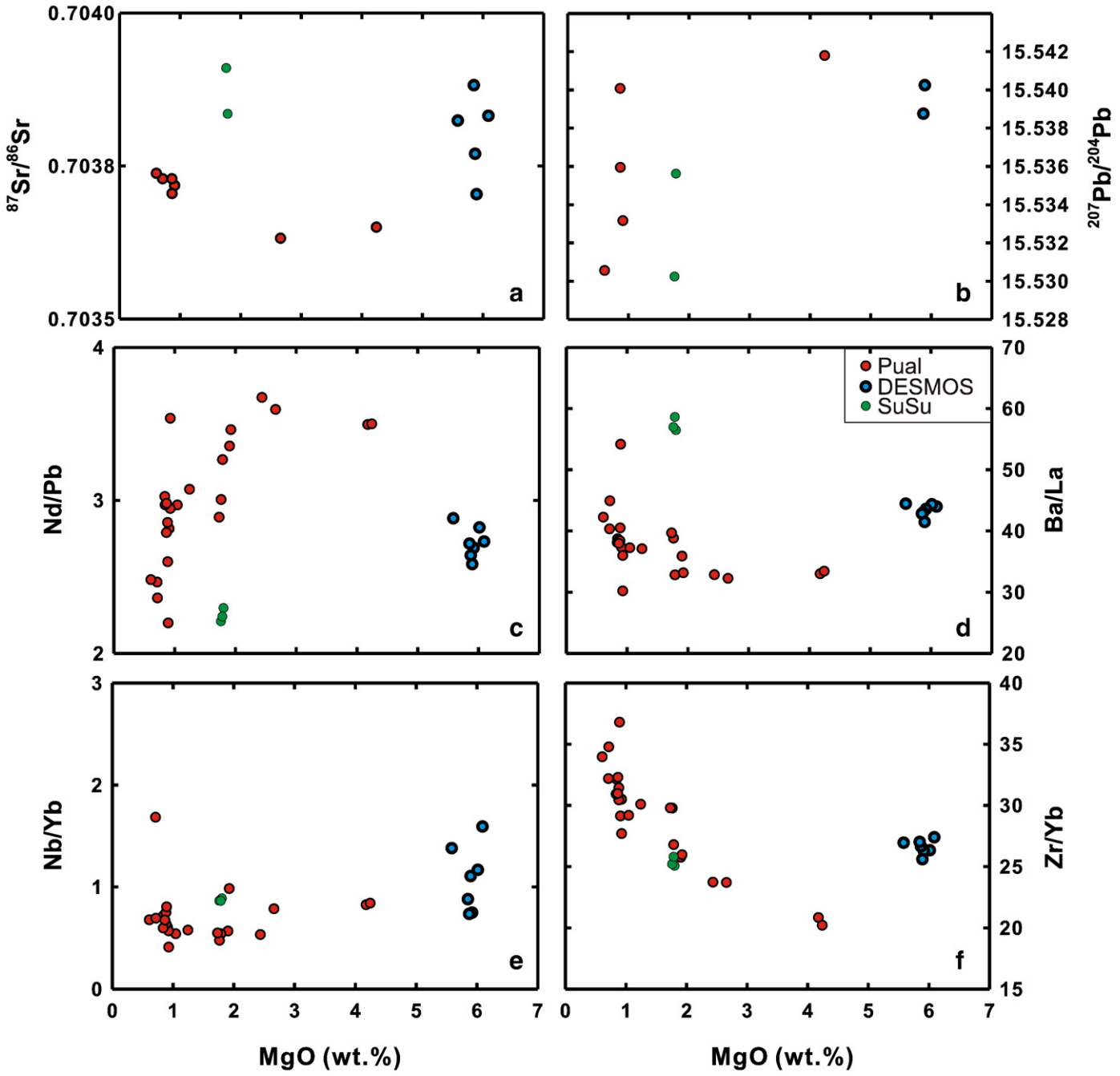

Fig. 6. a.$^{87}Sr/^{86}Sr$ versus MgO diagram. b. $^{207}Pb/^{204}Pb$ versus MgO diagram. c–f. Selected incompatible element ratios versus MgO diagrams.

Solomon and Pacific slab, respectively. Detailed examination of the presented data, however, reveals that the subduction components in SER lava came from the early subduction of the Pacific plate. For instance, the amount of the subduction component decreases with increasing distance from the New Ireland. On the other hand, such kind of relationship could not be observed as a function of distance from the New Britain. SER lavas may have been derived from the mantle lithosphere which accumulated subduction components during the active volcanic activity on New Ireland. Quantitative examination of Sr–Nd–Pb isotopic differences between the SER and TLTF lavas indicates that the SER lavas contain little sediment components and less MORB fluid than the TLTF lavas. Such findings are probably related with the difference in the tectonic setting as the SER was located in backarc whereas the TLTF was located in forearc during the former subduction of the Pacific slab. During active subduction of the Pacific slab, most of the sediment material above the slab was probably removed in the forearc section. As a result, less to none of the sediment material was available for introduction to the source of the SER mantle. MORB fluid can be effectively delivered into sub-forearc than backarc by shallow dehydration processes.

Acknowledgements

We would like to express our gratitude to the captain and crew of R/V Onnuri for their effort. We appreciate Jong-Ik Lee at Korea Polar Research Institute (KOPRI) and Seok-Hyun Kim at Korea Ocean Research and Development Institute (KORDI) for their help with XRF and ICP-MS analysis, respectively. We also appreciate David Christie at University of Alaska, Fairbanks for his constructive review of earlier draft, and comments made by Editor Dr. Bernard Bourdon and two anonymous

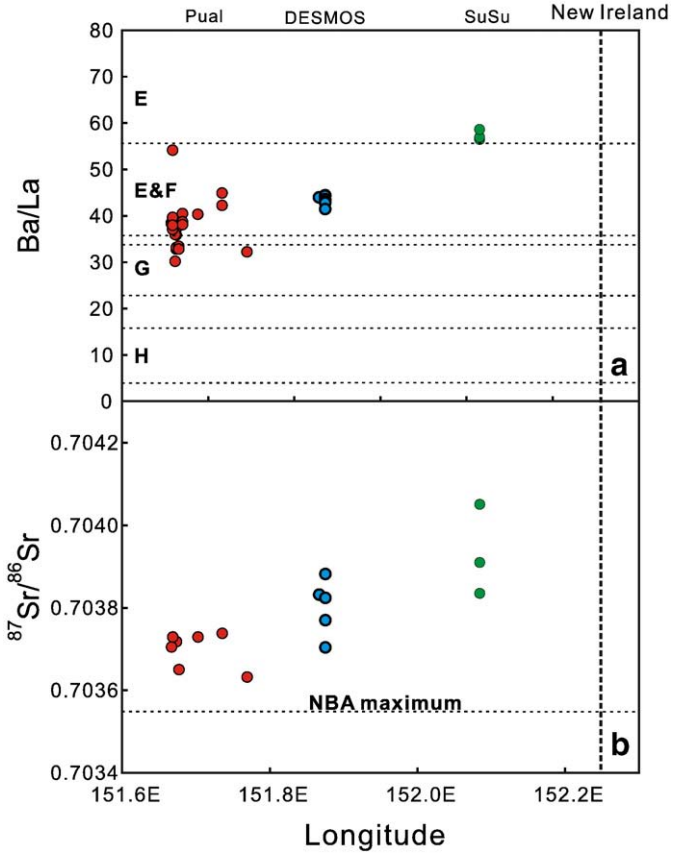

Fig. 7. Longitudinal variation of Ba/La (a) and $^{87}Sr/^{86}Sr$ (b). Note that both ratios are decreasing with away from New Ireland. Note also that Ba/La variation in SER lava is higher than zone G and covers the range of data from E and F (Fig. 1).

reviewers. This work which began as a part of the PhD thesis of Sung-Hyun Park at Seoul National University was finalized with the support of KOPRI (grant number PE09020). This work was also supported by the National Research Foundation (NRF) grant funded by the Korea government (MEST) (No. 2009-0092790).

References

Abbott, L.D., Silver, E.A., Thompson, P.R., Filewicz, M.V., Schneider, S., Abdoerrias, 1994. Stratigraphic constraints on the development and timing of arc-continent collision in northern Papua New Guinea. J. Sediment. Res. B64, 169–183.

Binns, R.A., Scott, S.D., 1993. Actively forming polymetallic sulfide deposits associated with felsic volcanic rocks in the eastern Manus back-arc basin, Papua New Guinea. Econ. Geol. 88, 2226–2236.

Class, C., Miller, D.M., Goldstein, S.L., Langmuir, C.H., 2000. Distinguishing melt and fluid subduction components in Umnak volcanics, Aleutian arc. Geochem. Geophys. Geosys. 1999GC000010.

DePaolo, D.J., 1981. Trace element and isotopic effects of combined wallrock assimilation and fractional crystallization. Earth Planet. Sci. Lett. 53, 189–202.

Fryer, P., Sinton, J.M., Philpotts, J.A., 1981. Basaltic glasses from the Marian Trough. In: Hussong, D.M., Uyeda, S., et al. (Eds.), Initial Reports of the Deep Sea Drilling Project, 60. US Government Printing Office, Washington DC, pp. 601–609.

Gena, K., Mizuta, T., Ishiyama, D., Urab, T., 1997. Geochemical characteristics of altered basaltic andesite by sulfuric-acid rich solution from the DESMOS caldera, Manus Basin, Papua New Guinea. JAMSTEC J. Deep Sea Res. 13, 269–285.

Gill, J.B., 1981. Orogenic andesites and plate tectonics. Springer, New York. 390 pp.

Hart, S.R., 1984. A large-scale isotope anomaly in the Southern Hemisphere mantle. Nature 309, 753–797.

Hickey-Vargas, R., Hergt, J.M., Spadea, P., 1995. The Indian Ocean-type isotopic signature in western Pacific marginal basins: origin and significance. In: Taylor, B., Natland, J. (Eds.), Active margins and marginal Basins of the Western Pacific: Am. Geophys. Union Geophys. Monogr. Ser., vol. 88, pp. 175–197.

Hofmann, A.W., 1997. Mantle geochemistry: the message from oceanic volcanism. Nature 385, 219–229.

Hofmann, A.W., Jochum, K.P., Seufert, M., White, W.M., 1988. Nb and Pb in oceanic basalts: new constrains on mantle evolution. Earth Planet. Sci. Lett. 79, 33–45.

Irvine, T.N., Baragar, W.R.A., 1971. A guide to the chemical classification of the common volcanic rocks. Can. J. Earth Sci. 8, 523–548.

Johnson, R.W., 1977. Distribution and major element chemistry of late Cenozoic volcanoes at the southern margin of the Bismarck Sea, Papua New Guinea. Australian Bureau of Mineral Resources Report 188.

Kamenov, G.D., Perfit, M.R., Jonasson, I.R., Mueller, P.A., 2005. High-precision Pb isotope measurements reveal magma recharge as a mechanism for ore deposit formation: Examples from Lihir island and Conical seamount, Papua New Guinea. Chem. Geol. 219, 131–148.

Kamenov, G.D., Perfit, M.R., Mueller, P.A., Jonasson, I.R., 2008. Controls on magmatism in an island arc environment: study of lavas and sub-arc xenoliths from the Tabar–Lihir–Tanga–Feni island chain, Papua New Guinea. Contrib. Mineral. Petrol. 155, 635–656.

Kennedy, A.K., Hart, S.R., Frey, F.A., 1990. Composition and isotopic constraints on the petrogenesis of alkaline arc lavas: Lihir Island, Papua New Guinea. J. Geophys. Res. 95, 6926–6942.

Kroenke, L., 1984. Ceonozoic tectonic development of the southwest Pacific. U.N. ESCAP, CCOP/SOPAC. Tech. Bull. 6 126 pp.

Langmuir, C.H., Bezos, A., Escrig, S., Parman, S.W., 2006. Chemical systematics and hydrous melting of the mantle in back-arc basin. In: Chirstie, D.M., Fisher, C.R., Lee, S.-M., Givens, S. (Eds.), Back-Arc Spreading Systems, Geological, Biological, Chemical, and Physical Interactions: Geophys. Monogr. Ser., vol. 166, pp. 87–146.

Le Maitre, R.W., Bateman, P., Dudek, A., Keller, J., Lameyre, J., Le Bas, M.J., Sabine, P.A., Schmid, R., Sorensen, H., Streckeisen, A., Woolley, A.R., Zanettin, B., 1989. A Classification of igneous rocks and glossary of terms: recommendations of the international union of geological sciences subcommission on the systematics of igneous rocks. Blackwell, Oxford.

Lee, S.-M., Ruellan, E., 2006. Tectonic and magmatic evolution of the Bismarck Sea, Papua New Guinea: review and new synthesis. In: Chirstie, D.M., Fisher, C.R., Lee, S.-M., Givens, S. (Eds.), Back-Arc Spreading Systems, Geological, Biological, Chemical, and Physical Interactions: Geophys. Monogr. Ser., vol. 166, pp. 263–286.

Martinez, F., Taylor, B., 1996. Backarc spreading, rifting, and microplate rotation, between transform faults in the Manus Basin. Mar. Geophy. Res. 18, 203–224.

McInnes, B.I.A., Cameron, E.M., 1994. Carbonated, alkaline hybridizing melts from a sub-arc environment: mantle wedge samples from Tabar–Lihir–Tanga–Feni arc, Papua New Guinea. Earth Planet. Sci. Lett. 122, 125–141.

McInnes, B.I.A., Gregoire, M., Binns, R.A., Herzig, P.M., Hannington, D., 2001. Hydrous metasomatism of oceanic sub-arc mantle, Lihir, Papua New Guinea: petrology and geochemistry of fluid-metasomatised mantle wedge xenolith. Earth Planet. Sci. Lett. 191, 1–5.

Miller, D.M., Goldstein, S.L., Langmuir, C.H., 1994. Ce/Pb and Pb isotope ratios in arc magmas and the enrichment of Pb in the continents. Nature 368, 514–519.

Othman, D.B., White, W.M., Patchett, J., 1989. The geochemistry of marine sediments, island arc magma genesis, and crust-mantle recycling. Earth Planet. Sci. Lett. vol. 94, 1–21.

Pearce, J.A., Peate, D.W., 1995. Tectonic implications of the composition of volcanic arc magmas. Annu. Rev. Earth Planet. Sci. 23, 251–285.

Pearce, J.A., Stern, R.J., Bloomer, S.H., Fryer, P., 2005. Geochemical mapping of the Mariana arc-basin system: Implications for the nature and distribution of subduction components. Geochem. Geophys. Geosyst. doi:10.1029/2004GC000895.

Pearce, J.A., Stern, R.J., Pearce, J.A., Stern, R.J., 2006. In: Christie, D.M., Fisher, C.R., Lee, S.-M., Givens, S. (Eds.), Back-Arc Spreading Systems, Geological, Biological, Chemical, and Physical Interactions: Geophys. Monogr. Ser., vol. 166, pp. 63–86.

Rickwood, P.C., 1989. Boundary lines within petrologic diagrams which use oxides of major and minor elements. Lithos 22, 247–263.

Salters, V.J.M., Stracke, A., 2004. Composition of the depleted mantle. Geochem. Geophys. Geosyst. 5.

Sinton, J.M., Ford, L.L., Chappell, B., McCulloch, M.T., 2003. Magma genesis and mantle heterogeneity in the Manus back-arc basin, Papua New Guinea. J. Petrol. 44, 159–195.

Staudigel, H., Davis, G.R., Hart, S.R., Marchant, K.M., Smith, 1995. Large scale isotopic Sr, Nd and O isotopic anatomy of altered oceanic crust: DSDP/ODP sites 417/418. Earth Planet. Sci. Lett. 130, 169–185.

Stracke, A., Hegner, E., 1998. Rifting-related volcanism in an oceanic post-collisional setting: the Tabar–Lihir–Tanga–Feni (TLTF) island chain, Papua New Guinea. Lithos 45, 545–560.

Sun, S.S., McDonough, W.F., 1989. Chemical and isotopic systematics of oceanic basalts: Implication for mantle composition and processes. In: Saunders, A.D., Norry, M.J. (Eds.), Magmatism in the oceanic basins: Geol. Soc. Lond. Spec. Publ., vol. 2, pp. 313–345.

Taylor, B., Martinez, F., 2003. Back-arc basin basalt systematics. Earth Planet. Sci. Lett. 210, 489–497.

Taylor, B., Crook, K.A.W., Sinton, J.M., 1994. Extentional transform zones and oblique spreading centers. J. Geophys. Res. 99, 19,709–19,718.

Wallace, L., Stevens, C., Silver, E., McCaffrey, R., Loratung, W., Hasiata, S., Stanaway, R., Curley, R., Rosa, R., Taugaloid, J., 2004. GPS and seismological constraints on active tectonics and arc-continent collision in Papua New Guinea: Implications for mechanisms of microplate rotations in a plate boundary zone. J. Geophys. Res. 109. doi:10.1029/2003JB002481.

Woodhead, J.D., Johnson, R.W., 1993. Isotope and trace element profiles across the New Britain island arc, Papua New Guinea. Contrib. Mineral. Petrol. 113, 479–491.

Woodhead, J.D., Eggins, S.M., Johnson, R.W., 1998. Magma genesis in the New Britain Island arc: further insights into melting and mass transfer processes. J. Petrol. 39, 1641–1668.